ChemPubSoc Europe

DOI: 10.1002/chem.201602141

CHEMISTRY A European Journal Full Paper

Photocatalysis |Hot Paper|

Enhanced Photocatalytic Performance of ZnO Nanorods Coupled by Two-Dimensional α-MoO_3 Nanoflakes under UV and Visible Light Irradiation

Da-Ren Hang,*[a] Krishna Hari Sharma,[a] Chun-Hu Chen,[b] and Sk Emdadul Islam[a]

Abstract: We exploit the utilization of two-dimensional (2D) molybdenum oxide nanoflakes as a co-catalyst for ZnO nanorods (NRs) to enhance their photocatalytic performance. The 2D nanoflakes of orthorhombic α-MoO_3 were synthesized through a sonication-aided exfoliation technique. The 2D MoO_3 nanoflakes can be further converted to substoichiometric quasi-metallic MoO_{3-x} by using UV irradiation. Subsequently, 1D–2D MoO_3/ZnO NR and MoO_{3-x}/ZnO NR composite photocatalysts have been successfully synthesized. The photocatalytic performances of the novel nanosystems in the decomposition of methylene blue are studied by using UV- and visible-illumination setup. The incorporated 2D nanoflakes show a positive influence on the photocatalytic activity of the ZnO. The obtained rate constant values follow the order of pristine ZnO NR < MoO_3/ZnO NR < MoO_{3-x}/ZnO NR composites. The enhancement of the photocatalytic efficiency can be ascribed to a fast charge carrier separation and transport within the heterojunctions of the MoO_3/ZnO NRs. In particular, the best photocatalytic performance of the MoO_{3-x}/ZnO NR composite can be additionally attributed to a quasi-metallic conductivity and substoichiometry-induced mid-gap states, which extend the light absorption range. A tentative photocatalytic degradation mechanism was proposed. The strategy presented in this work not only demonstrates that coupling with nanoscale molybdenum oxide nanoflakes is a promising approach to significantly enhance the photocatalytic activity of ZnO but also hints at new type of composite catalyst with extended applications in energy conversion and environmental purification.

Introduction

Green technology, such as disposing of industrial wastewater, energy storage, and conversion, is central to the present needs of our ecosystem and society. The use of semiconductor photocatalysts, such as TiO_2 and zinc oxide (ZnO), for the degradation of organic pollutants and clean hydrogen production, have attracted considerable attention over the past years.[1,2] In particular, ZnO is a versatile semiconductor platform for various applications in optoelectronics, sensors, and photocatalysis owing to its high photosensitivity, non-toxicity, stability, and diverse nanostructures.[3–5] Among various morphologies, one-dimensional (1D) ZnO nanorods (NRs) are a suitable form for photocatalysis due to their merits: 1) large surface area for efficient mass transfer and reactant access, 2) retaining the ease of a consecutive usage of the NR substrates, and 3) various cost-effective synthesis routes. At present, two limiting factors for photocatalytic processes of ZnO NRs are considered. The first one is the strong recombination of photogenerated charge carriers, which reduces the photocatalytic efficiency; the second one is the low photon utilization efficiency in visible light. Various strategies have been developed to overcome these limitations, such as doping with transition-metal ions,[6] loading with noble-metal co-catalysts,[7–11] and compositing with other semiconductors.[12] Noble metals, such as Pt, have been proven to be very efficient co-catalysts but the high material costs make their practical use rather limited.[13] Consequently, it is essential to develop noble-metal-free co-catalysts for ZnO NRs.

Recently, the exploitation of two-dimensional (2D) layered materials for the application in photocatalysis has gained increasing interest.[14,15] Graphene, the most studied 2D nanosheet, is noted for a superior electron mobility because of the 2D π-conjugated structure, which facilitates the electron transfer and separation of the photogenerated charge carriers.[14] However, graphene has a weak visible-light absorption efficiency, so it does not significantly improve the light-harvesting capability of graphene-based hybrid photocatalysts. In addition, it was found that graphene has low activation ability for H_2 production. The quest for 2D layered photocatalysts with a non-zero band gap has driven the exploration of 2D transition-metal dichalcogenides and molybdenum trioxide.[16,17] In the past few years, molybdenum disulfide (MoS_2) was inten-

[a] Prof. D.-R. Hang, K. H. Sharma, S. E. Islam
Department of Materials and Optoelectronic Science
National Sun Yat-sen University, 70 Lienhai Rd.
Kaohsiung 80424 (Taiwan)
E-mail: drhang@faculty.nsysu.edu.tw

[b] Prof. C.-H. Chen
Department of Chemistry, National Sun Yat-sen University
70 Lienhai Rd., Kaohsiung 80424 (Taiwan)

Supporting information for this article and ORCID for one of the authors are available on the WWW under http://dx.doi.org/10.1002/chem.201602141.

sively studied for electronics, photonics, and catalysis.[16] However, previous studies have concluded that the catalytic activity of the thermodynamically stable 2H (trigonal-prismatic) phase of MoS_2 arises from the metallic edges, whereas its semiconducting basal surface is catalytically inert.[18,19] Adoption of a high aspect ratio and a high surface area nanostructure can increase the activity efficiency, but the conductivity of MoS_2 is poor along certain crystallographic directions, posing more limitation to the design of high surface area structures. Furthermore, the mobility of the semiconducting 2H phase of MoS_2 is rather limited for charge transport. To avoid these shortcomings, several current works proposed the use of the metastable metallic 1T (octahedral) phase of MoS_2 to improve its catalytic activity.[20,21] On the other hand, a new perspective on the 2D layered catalytic materials beyond graphene can be unfolded by considering 2D few-layered MoO_3 nanoflakes. The stable orthorhombic α-phase of MoO_3 has a peculiar dual layer structure in which adjacent double layers of connected distorted MoO_6 octahedra are linked by weak van der Waals forces. Within each double layer the atoms are mainly connected by strong covalent and ionic bonding. Its electronic properties can be tuned by several ways. It was found that oxygen vacancies can induce mid-gap states that, in turn, narrow the optical band gap. More free electrons are released from reduced Mo ions, leading to a change in the conductivity from semiconducting to quasi metallic. Furthermore, MoO_3 provides a high κ environment to boost the carrier mobility by reducing Coulombic scattering. It was shown that the mobility of a reduced α-phase MoO_3-based field effect transistor (FET) exceeds the mobility value of silicon.[22] Therefore 2D layered MoO_3 should be a promising material to explore the photocatalytic enhancement.

To obtain mono- and few-layered materials, micro-mechanical and liquid-phase exfoliation methods are two major preparation techniques. Mechanical exfoliation is capable of delivering nanosheets with high crystal quality, but the yield is poor. The liquid-phase exfoliation technique shows a great potential to produce 2D nanosheets in large quantity and it is a practical way to facilitate various applications of 2D materials. Based on the scalable and reliable production of 2D nanosheets by liquid-phase exfoliation, we propose that 2D few-layer α-MoO_3 nanoflakes can be used in hybrid form to promote the photocatalytic performance of ZnO NRs. In this paper, we demonstrate the fabrication of photocatalytic nanocomposite structures where ZnO NRs are coupled by 2D few-layer α-MoO_3 nanoflakes. The ZnO NRs act as a 1D photocatalytic semiconductor to generate photoexcited electrons that are subsequently separated from the holes and transferred to the α-MoO_3 nanoflakes for photocatalytic reactions. The hybrid structures exhibit an improved performance to bare ZnO NRs in the photocatalytic degradation of methyl blue (MB) in both the UV and visible spectral range. In addition, it is found that substoichiometric 2D molybdenum oxide flakes as co-catalyst can provide a superior photocatalytic performance. As far as we know, this is the first example to use 2D α-MoO_3 nanoflakes as a co-catalyst for ZnO in photocatalytic applications. The presented 1D–2D nanocomposite structures provide new versatile and cost-effective platforms for future photocatalytic, sensing, and optical applications.

Results and Discussion

X-ray diffraction patterns of the as-synthesized 2D MoO_3 and MoO_{3-x} nanoflakes deposited on Si substrates are displayed in Figure S1 in the Supporting Information. The most intense peak at about 29° is attributed to the Si (111) substrate. We can identify reflections from (110), (020), (040), and (060) planes of the orthorhombic molybdenum trioxide (α-MoO_3) crystal structure. Figure 1 shows the XRD patterns of pristine ZnO NRs, MoO_3/ZnO, and MoO_{3-x}/ZnO nanocomposites. The peak located at 34.53 and 72.66° in the pristine ZnO NRs is attributed to the (002) and (004) plane of a ZnO wurtzite crystal. In the cases of the MoO_3/ZnO and MoO_{3-x}/ZnO nanocomposites, an extra peak is revealed at 26.9°, which is ascribed to the (040) plane of the α-MoO_3 structure.

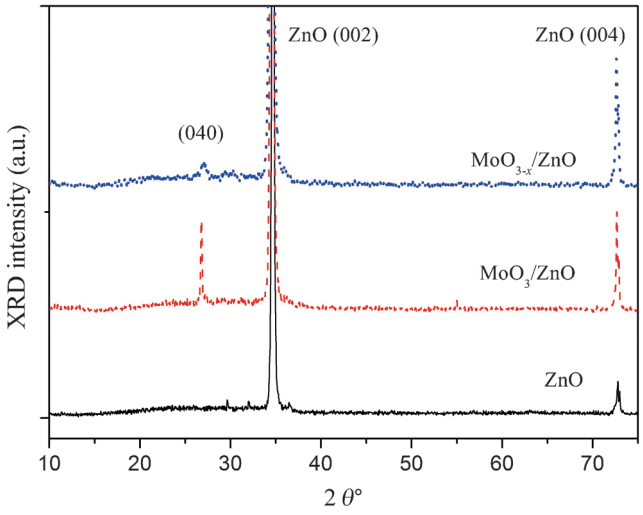

Figure 1. XRD θ–2θ scan of the as-prepared samples including pristine ZnO NRs as well as the MoO_3/ZnO and MoO_{3-x}/ZnO composites.

To investigate the structural properties of the as-prepared 2D MoO_3 nanoflakes, TEM measurements were carried out. Figure 2a shows typical TEM micrographs of the as-prepared MoO_3 nanoflakes. The electron transparency of the flakes indicates that the bulk MoO_3 was well exfoliated to very thin 2D nanosheets. High-resolution transmission electron microscopy (HRTEM) is utilized to further examine the quality and the crystal structure of the 2D MoO_3 nanoflakes. The HRTEM image in Figure 2b confirms that the as-prepared 2D MoO_3 nanoflakes are composed of single-crystalline structures and are defect-free. The measured fringe spacing is 0.39 nm, which corresponds to the (100) plane of the orthorhombic phase of MoO_3. The regular rectangular diffraction dot lattice of the selected area electron diffraction (SAED) pattern also proves the single-crystalline nature of the as-prepared 2D MoO_3 nanoflakes, as shown in Figure 2c. Atomic force microscopy (AFM) topography is employed to assess the thickness of these 2D MoO_3

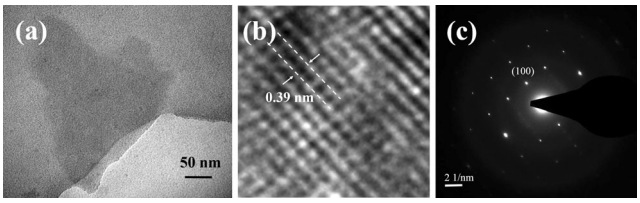

Figure 2. a) Representative TEM image of a MoO_3 nanoflake. b) HRTEM image of a 2D nanoflake and c) the corresponding SAED pattern.

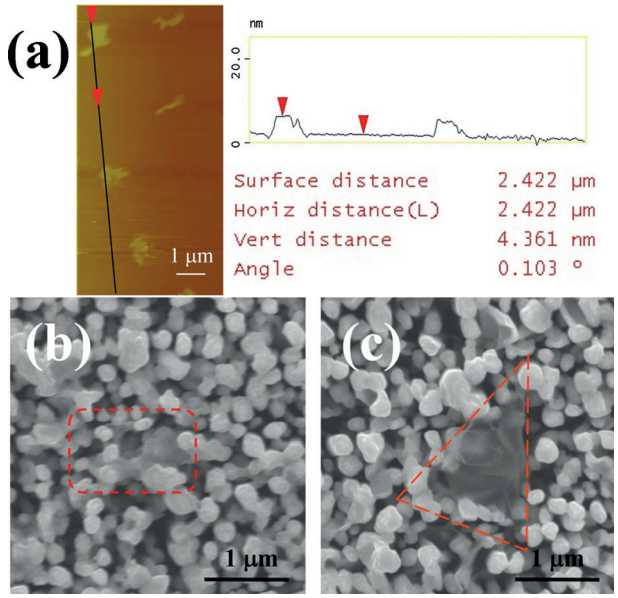

Figure 3. a) AFM image of MoO_3 nanoflakes and section height profile along the black line overlaid on the image. SEM images of composite samples b) MoO_3/ZnO and c) MoO_{3-x}/ZnO.

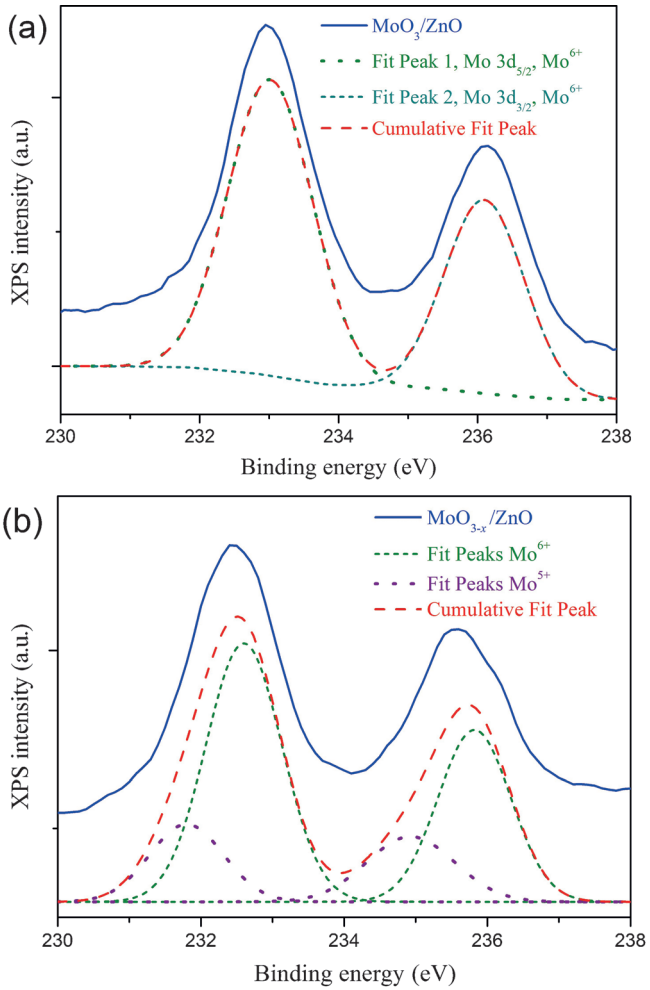

Figure 4. XPS spectra of the 2D molybdenum oxide flakes for the Mo 3d core level a) before and b) after exposure to UV illumination.

nanoflakes. Figure 3a shows the AFM image of liquid-exfoliated 2D MoO_3 nanoflakes deposited on a flat silicon wafer. As shown in the height profile of the AFM image, a step of 4.3 nm (corresponding to three fundamental dual layers of the α-MoO_3 structure) with an average lateral size of around 800 nm can be observed. Figures 3b and c present typical top-view SEM images of the MoO_3/ZnO and MoO_{3-x}/ZnO nanocomposites, respectively. First, the ZnO NRs are vertically aligned on an Al-doped zinc oxide (AZO) substrate with a high cover density. These ZnO NRs have an average diameter in the range of 100–150 nm. Importantly, it can be seen that the 2D MoO_3 (MoO_{3-x}) nanoflakes are located on the tips of the ZnO NRs, as highlighted by red dashed lines in Figures 3b and c.

The obtained nanocomposites were further investigated by XPS measurements to understand the chemical states of Mo. Figures 4a and b show the Mo 3d core level XPS spectra of the MoO_3/ZnO and MoO_{3-x}/ZnO nanocomposites, respectively. The Mo oxidation states present in the nanocomposites can be probed by checking the doublets of the binding energy. In Figure 4a, the Mo $3d_{5/2}$ and $3d_{3/2}$ peaks located at binding energies of 232.91 and 236.01 eV are attributed to the 6+ oxidation state of the MoO_3 phase, which dominates in the pristine 2D MoO_3 nanoflakes. The integral areas between the two doublets have a ratio of 2:3 and the energy gap between them is 3.1 eV, which is in agreement with a previous report.[23] After UV exposure, the Mo 3d peaks became broadened because of the appearance of the additional Mo^{5+} oxidation state, as shown in Figure 4b. Here, two sets of doublets are required to fit the data; the peaks at 235.8 and 232.6 eV correspond to the $3d_{3/2}$ and $3d_{5/2}$ of the Mo^{6+} core ions, whereas the peaks at 234.9 and 231.8 eV correspond to the $3d_{3/2}$ and $3d_{5/2}$ of the Mo^{5+} ions. The reduction of the Mo atoms from the 6+ state to the 5+ state is associated with oxygen vacancies. The additional electron of the Mo^{5+} ion relative to the Mo^{6+} ion can be delocalized so that the carrier concentration, and therefore the conductivity, can be enhanced. Another significant consequence of the introduction of Mo^{5+} states is the formation of gap states in the forbidden band.[24] Electrons in the gap states can be excited to the conduction band by means of a wide range of energy. It facilitates the extension of light absorption to the visible spectral region, thereby bringing about an enhancement of the photocatalytic efficiency.

Raman scattering measurements were carried out to understand the lattice dynamics. The Raman spectra of both MoO_3/ZnO and MoO_{3-x}/ZnO samples are presented in Figure 5a. For

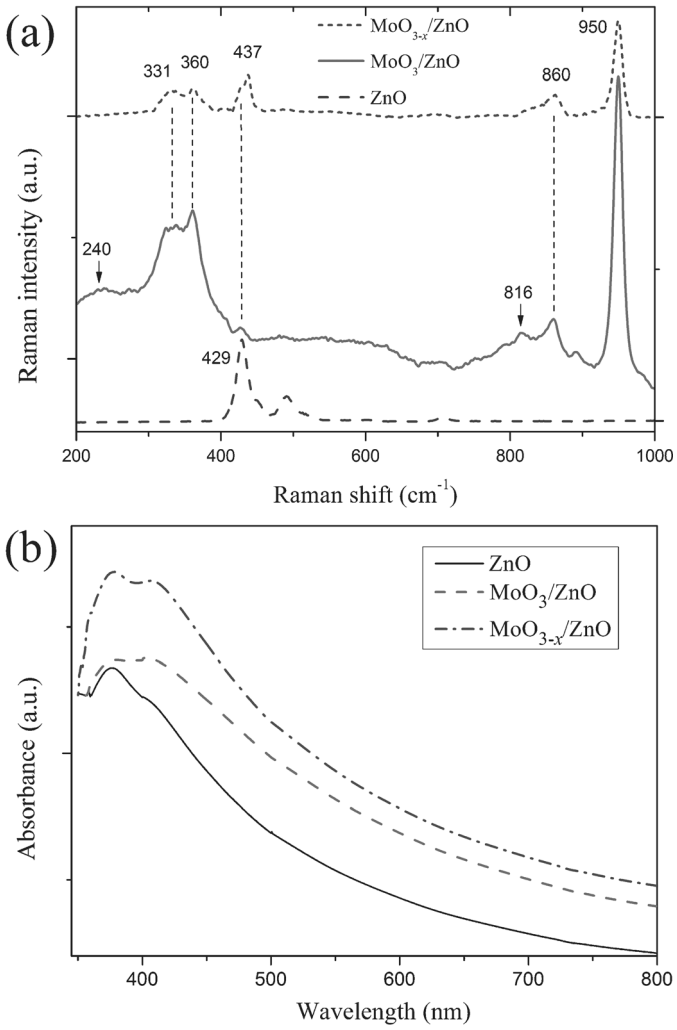

Figure 5. a) Raman spectra of pristine ZnO NRs as well as the MoO_3/ZnO and MoO_{3-x}/ZnO composites. b) The UV/Vis spectra of the ZnO NRs as well as the MoO_3/ZnO and MoO_{3-x}/ZnO composites.

comparison, the Raman spectrum of the ZnO NR substrate is also shown here, where the dominant peak at $\tilde{\nu}=429\ cm^{-1}$ is attributed to the E_2^H mode of the wurtzite ZnO structure.[25,26] The Raman peaks centered at $\tilde{\nu}=331$, 360, 429, 860, and 950 cm^{-1} were observed for both nanohybrids. The most intense peak at $\tilde{\nu}=950\ cm^{-1}$ originated from the terminal oxygen (Mo^{6+}=O) stretching mode, which is ascribed to an unshared oxygen atom of moderated hydrated MoO_3.[23,27–29] It was proposed that hydration of the MoO_3 occurs during the liquid-phase exfoliation process.[30] The peak at $\tilde{\nu}=860\ cm^{-1}$ represents the doubly coordinated oxygen (Mo_2O/Mo-O-Mo) stretching mode, which is related to corner-sharing oxygen atoms in common to two octahedral in slightly hydrated MoO_3. For MoO_3/ZnO, a shoulder at $\tilde{\nu}=816\ cm^{-1}$ represents the doubly coordinated oxygen symmetric stretching mode, which results from corner-shared oxygen atoms in common to two undistorted MoO_6 octahedra.[31,32] After UV irradiation, an additional Raman signal was further revealed at $\tilde{\nu}=437\ cm^{-1}$, which is related to the deformation modes of the (Mo–OH) bond.[27,33,34] Bands in the regime $\tilde{\nu}=300$–400 cm^{-1} are usually due to bending modes of MoO_6 octahedra. The peaks located at $\tilde{\nu}=331$ and 360 cm^{-1} can be attributed to triply coordinated oxygen (Mo_3–O) and the double-bond (Mo=O) bending modes, respectively. Finally, the weak shoulder appearing at $\tilde{\nu}=240\ cm^{-1}$ is related to the bending mode of Mo_2–O.[32]

Figure 5b shows the UV/Vis absorption spectra of pure ZnO NRs and the nanocomposites. The ZnO NRs exhibit an UV absorption band at $\lambda=377$ nm, which accords with a band-to-band transition. In the case of the MoO_3/ZnO and MoO_{3-x}/ZnO nanocomposites, another absorption band is clearly observed at $\lambda=410$ nm, which corresponds to the presence of 2D MoO_3 (or MoO_{3-x}) nanoflakes. We found that the absorption of the MoO_3/ZnO NR composites was improved in the UV and visible spectrum due to the existence of MoO_3 that modified the optical absorption properties. In addition, as we replace the 2D co-catalyst MoO_3 by MoO_{3-x} flakes, the absorption intensities of the composite were further enhanced. Thus, it is expected that the photocatalytic activity can be enhanced compared with that of pristine ZnO NRs.

The photoluminescence (PL) properties are closely related to the trapping, immigration and the recombination of photogenerated electrons–hole pairs in semiconductors. The room-temperature PL spectra in the near-band-edge (NBE) range of our photocatalysts are shown in Figure 6. As expected, the NBE band centered at 3.28 eV of the pristine ZnO NRs mainly originated from the free exciton recombinations from the ZnO NRs.[25,35] For both composite samples, the PL bands are similar to that of the pristine ZnO NRs, however, the PL intensities are apparently reduced. The suppression of the emission yield of composite photocatalysts may be attributed to the formation of a heterojunction between the ZnO NRs and the molybdenum oxide nanoflakes, which prevents recombination of photogenerated carriers efficiently. On the basis of the PL results, we may deduce that the order of the photocatalytic activity of the samples is MoO_{3-x}/ZnO > MoO_3/ZnO > pure ZnO, which can be further demonstrated by photocatalytic experiments described below.

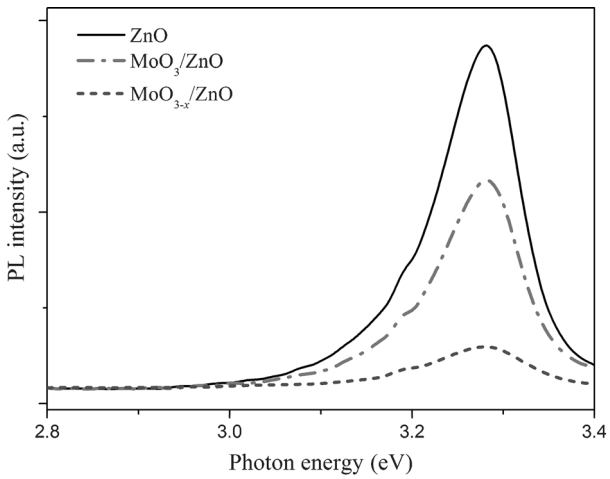

Figure 6. Photoluminescence spectra of the as-prepared ZnO NRs as well as the MoO_3/ZnO and MoO_{3-x}/ZnO composites.

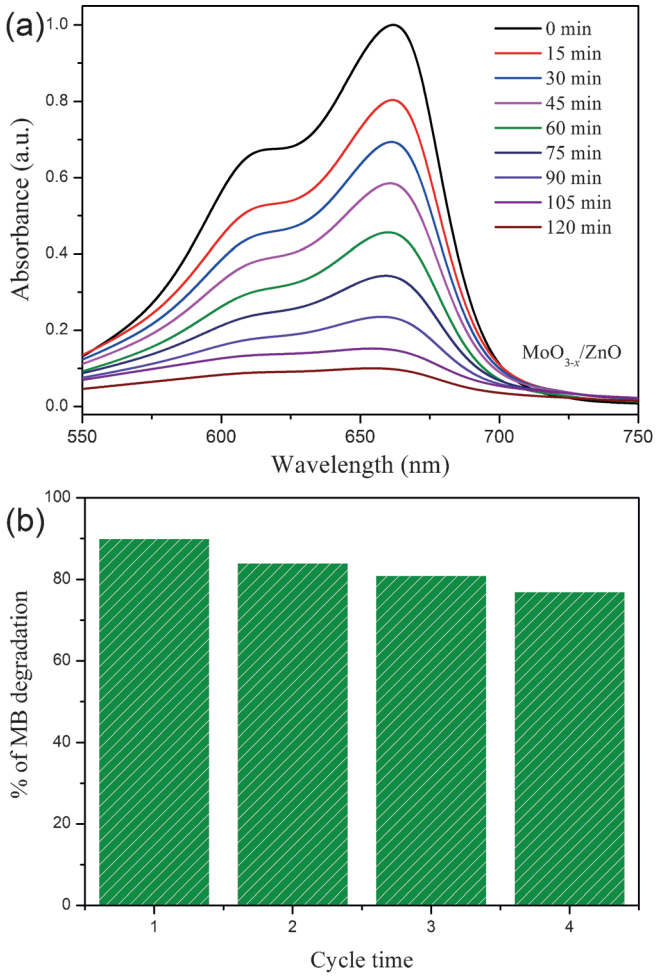

Figure 7. a) Time-dependent absorption spectra of a solution of MB under UV-light irradiation in the presence of the MoO_{3-x}/ZnO composite and b) the corresponding cycling runs up to four times in the photocatalytic degradation of MB.

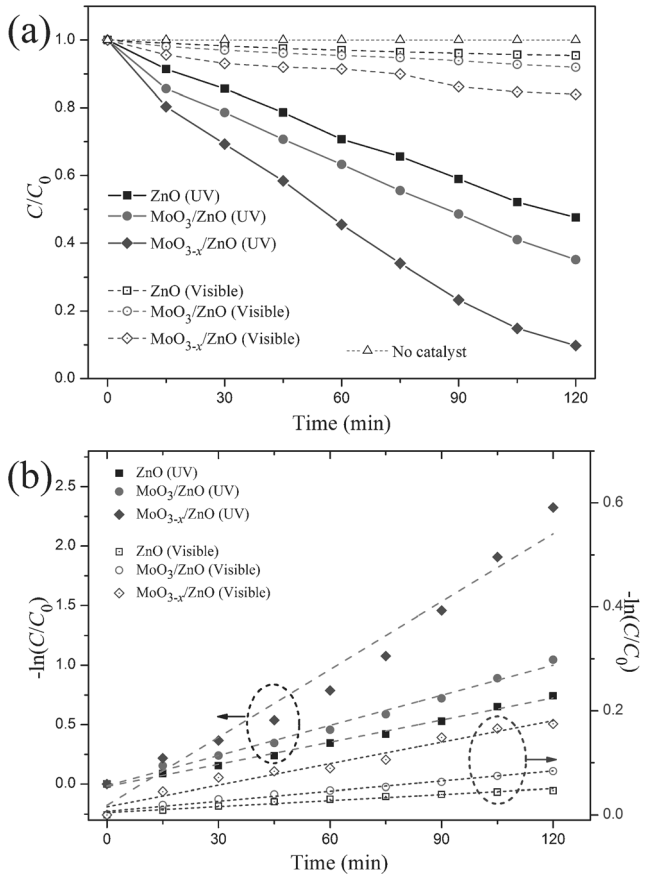

Figure 8. a) Degradation rate of MB (C/C_0) as a function of the irradiation time under UV- and visible-light irradiation and (b) the corresponding plots of $-\ln(C/C_0)$ versus t of pristine ZnO NRs as well as the MoO_3/ZnO and MoO_{3-x}/ZnO composites.

Photocatalytic experiments were carried out by using the degradation reaction of methyl blue under UV-light irradiation. We found that the MoO_{3-x}/ZnO composite photocatalyst showed the best photodegradation performance. Figure 7a displays the absorption spectra of a solution of MB in the presence of the photocatalyst MoO_{3-x}/ZnO. The characteristic absorption of MB at $\lambda = 662$ nm decreases progressively with an increase of the exposure time, and almost disappears after about 120 min. Figure 8a shows the photodegradation rates of MB by using the pristine ZnO NR catalysts and ZnO NR substrates loaded with 2D MoO_3 and MoO_{3-x} flakes. One can see that all the ZnO nanocomposite samples exhibit higher photocatalytic activities than the pristine ZnO NR sample. The photocatalytic kinetics can be concisely described by a pseudo-first-order reaction, that is, $C = C_0 \exp^{-kt}$, where C_0 and C are the initial concentration of MB at $t = 0$ and the concentration at the exposure time t, which correspond to the absorbance of MB at $\lambda = 662$ nm.[36] The apparent reaction rate constant k gives a quantitative measure of the photocatalytic kinetics. The k value can be estimated from a plot of $-\ln(C/C_0)$ versus t, and the results are summarized in Figure 8b. The pristine ZnO NRs possess an apparent reaction rate constant k of 0.0062 min^{-1}, whereas the sample of ZnO NRs hybridized with 2D MoO_3 flakes raises the apparent reaction rate constant to 0.0084 min^{-1}. In addition, the sample with the 2D MoO_{3-x} flakes showed the highest activity ($k = 0.01899$ min^{-1}), the activity of the degradation of MB was increased by more than three times after 2D MoO_{3-x} flakes were loaded. Next, we check the photocatalytic activity of pristine ZnO and the ZnO composite photocatalysts under visible-light irradiation, which is shown in Figure 8a (open symbols). The photocatalytic efficiency of pristine ZnO NRs is low with this visible illumination setup. Only about 4.6% of the dye could be degraded within 120 min in this case. Again, we found that the degradation rate of MB can be enhanced upon utilizing the 2D flakes as co-catalysts. As shown in Figure 8b, the k values of pristine ZnO, MoO_3/ZnO, and MoO_{3-x}/ZnO are 0.00038, 0.00064, and 0.00138 min^{-1}, respectively. The k value of MoO_{3-x}/ZnO is the highest, which is about 3.6 times higher than that of the pristine ZnO NRs. Therefore, our results demonstrate that the 2D MoO_3 and MoO_{3-x} nanoflakes can be used to enhance the photocatalytic efficiency of ZnO NRs in any case we studied. The ZnO NR-based substrate provides a platform, which is facile for repeated use. To check the stability of the photocatalytic performance, the MoO_{3-x}/ZnO nanocomposite was used to de-

grade the MB dye in four consecutive cycles, as shown in Figure 7b. It was found that after four cycles for the photodegradation, the photocatalyst did not exhibit a substantial loss of activity, which reveals that the MoO_{3-x}/ZnO photocatalyst has a good stability.

On the basis of the above-described results, the photocatalytic mechanism for the MoO_3/ZnO and MoO_{3-x}/ZnO nanocomposites is tentatively proposed and schematically illustrated in Scheme 1. Under UV-light irradiation, both ZnO and MoO_3 can be excited to induce the formation of photogenerated electrons and holes (Scheme 1a). The electrons in the conductive band (CB) of the ZnO could easily transfer to the CB of MoO_3 because the CB position of MoO_3 was lower than that of ZnO. The delocalized electrons can induce various degradation reactions, notably by forming the superoxide anion ($O_2^{\bullet-}$), hydroperoxyl ($HO^{\bullet}_2$), and hydrogen peroxide (H_2O_2). Because the CB potential of MoO_3 [+0.40 V vs. normal hydrogen electrode (NHE)] was lower than the standard redox potential of $O_2^{\bullet-}/O^{\bullet}_2$, direct formation of $O_2^{\bullet-}$ (−0.33 V vs. NHE) and hydroperoxyl (−0.046 V vs. NHE) will be difficult. Therefore, the photoelectrons in the CB of MoO_3 would be transferred to hydrogen peroxide through the processes described in Equation (1).[37]

$$O_2+2H^++2e^- \rightarrow H_2O_2 \qquad E_0 = +0.682\,V \tag{1}$$

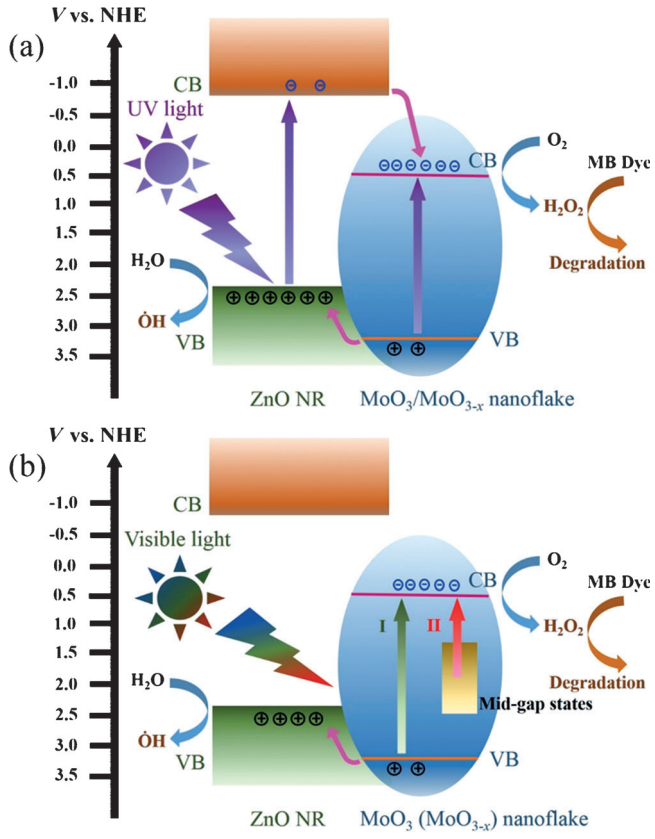

Scheme 1. Schematic diagrams showing the energy band structure and transitions of the MoO_3/ZnO and MoO_{3-x}/ZnO composites under a) UV- and b) visible-light irradiation. Possible schemes for charge carrier generation, transfer, and degradation of the dye are illustrated.

At the same time, the photogenerated holes in the valence bond (VB) of MoO_3 will be transported to that of ZnO. Because of the double charge-transfer mechanism, the recombination of the photogenerated electrons and holes is suppressed, which is evidenced by our PL results.[38,39] The accumulation of holes in the VB of ZnO leads to the formation of $OH^{\bullet}$ radicals through Equations (2) and (3).[40,41] The generated $OH^{\bullet}$ radicals are very powerful oxidant so the organic dyes can be efficiently degraded by these radicals.

$$H_2O+h^+ \rightarrow H^++OH^{\bullet} \qquad E_0 = +1.99\,V \tag{2}$$

$$OH^-+h^+ \rightarrow OH^{\bullet} \qquad E_0 = +2.72\,V \tag{3}$$

Under visible-light irradiation, the photodegradation efficiency is lower than that under UV-light irradiation. In this case, the number of mobile charge carriers from band-to-band transitions in the majority of the ZnO NR structure is rather small. Photogenerated electrons and holes can be excited in the 2D MoO_3 nanoflakes for subsequent degradation processes, as shown by transition I in Scheme 1b. So the photodegradation efficiency can be increased by incorporating 2D MoO_3 nanoflakes. For the 2D MoO_{3-x} nanoflakes, a large number of oxygen vacancies exists, leading to the formation of a mid-gap band.[24] These states are responsive to visible-light irradiation, as represented by transition II in Scheme 1b. Together with the quasi-metallic surface conductivity properties, the MoO_{3-x}/ZnO nanocomposite photocatalyst has a substantial enhancement in the photocatalytic activity compared with the pristine ZnO NR photocatalyst. Our results indicate that 2D MoO_3 and MoO_{3-x} nanoflakes can be used in composite form with wide band-gap semiconductors to strengthen the photocatalytic efficiency both under UV- and visible-illumination conditions.

Conclusion

1D–2D MoO_3/ZnO and MoO_{3-x}/ZnO composite photocatalysts have been proposed and were successfully prepared by employing hydrothermal and liquid-phase exfoliation methods. The 2D nanoflakes of α-MoO_3 were synthesized through the sonication-aided exfoliation technique. These few-layer nanoflakes have a nanoscale thickness and were highly crystalline as evidenced by AFM and HRTEM. The properties and stoichiometry of the 2D α-MoO_3 nanoflakes can be further modified by irradiation with UV light. Subsequently, these 2D molybdenum oxide nanoflakes were incorporated to fabricate 2D nanoflake/1D NR composite photocatalysts. The electron–hole recombination for the nanoflake/ZnO NR heterojunction was significantly reduced in comparison with pure ZnO NRs, indicating the efficient separation of photogenerated charge carriers in the composite nanostructures. The introduced 2D molybdenum oxide nanoflakes show a substantial positive influence on the photocatalytic reaction rate constant. By performing a photocatalytic experiment, we found that the MoO_{3-x}/ZnO composite shows the best photocatalytic degradation efficiency under both visible- and UV-light irradiation. The superior photocatalytic performance can be further attributed to quasi-met-

allic conductivity and substoichiometry-induced mid-gap states, which strengthens the visible-light-harvesting efficiency. The proposed 2D nanoflake/ZnO NR substrate provides a platform that can be easily separated and recycled. After four successive degradation cycles, the composite is fairly stable under the studied conditions. Our results show that coupling with nanometer-thick oxide nanoflakes is a promising approach to significantly enhance the photocatalytic activity of ZnO and the substoichiometry of oxide nanoflakes provides a novel route to optimize the photocatalytic efficiency.

Experimental Section

Synthesis of molybdenum oxide nanoflakes

Molybdenum oxide powder (1 g) (from Sigma—Aldrich) was ground with ethylenediamine (200 μL) for 30 min before being mixed with water and ethanol (1:1, v/v), which is analogous to a previously reported paper.[27] Then the solution was probe-sonicated for 120 min at a power of 200 W and centrifuged at 6000 rpm. Afterwards, the supernatant containing the 2D MoO_3 nanoflakes was divided in two parts. One part is used as pristine MoO_3 nanoflakes and the other part was transformed to reduced molybdenum oxide (MoO_{3-x}) nanoflakes by exposure to irradiation from a 600 W xenon lamp (Newport, USA) for 600 min.

Synthesis of the MoO_3/ZnO and MoO_{3-x}/ZnO nanocomposites

Al-doped zinc oxide (AZO) substrate was adopted for the growth of ZnO NRs, as reported in our previous paper.[26] In short, AZO substrates of 2×2 cm^2 dimensions were first cleaned by acetone and deionized water, and subsequent cleaning was provided by using an oxygen plasma for 60 s. Then, the AZO substrates were immersed in an aqueous solution of 0.1 M zinc nitrate hexahydrate ($Zn(NO_3)_2{\cdot}6H_2O$) and hexamethylenetetramine (HMTA), which was kept in a Teflon-coated autoclave. The autoclave was sealed and heated in an oven at 90 °C for 10 h. The ZnO substrate was finally taken out of the solution and then rinsed several times and dried for further use. As 2D MoO_3 and MoO_{3-x} nanoflakes were dispersed in solvent, an aliquot (500 μL) of each solution was drop-casted on different ZnO NR substrates. Then the nanocomposite substrates were kept overnight at 60 °C.

Instruments and measurements

X-ray diffraction (XRD) patterns were recorded by using a Siemens D5000 diffractometer. The surface morphology of the nanocomposites was examined by using field emission scanning electron microscopy (FESEM, JEOL 6330). The TEM image of the 2D MoO_3 nanoflakes was captured by using a Philip CM 200 instrument. The surface chemical states were probed by using X-ray photoelectron spectrometer (XPS, JEOL JPS-9010). The thickness of the 2D nanoflakes was evaluated by atomic force microscopy (AFM, Digital instruments Nanoscope). Raman measurements were performed in a backscattering configuration on a micro-Raman setup by using a $\lambda = 633$ nm laser. Absorbance measurements were done with a Thermo Evolution 201 UV/visible spectrophotometer. The photoluminscence (PL) measurements were carried out by using a He/Cd (Kimmon, IK series) laser with an excitation wavelength of $\lambda =$ 325 nm at room temperature.

Photocatalytic tests

Methylene blue, having the molecular formula $C_{16}H_{18}N_3SCl$, is one of the frequently used dyes in industry. The photodegradation of MB was chosen as a model reaction to evaluate the photocatalytic activity of our samples under UV- and visible-light irradiation. The photocatalytic activity for the pristine ZnO NRs and the nanocomposite samples were performed in a quartz vessel containing an aqueous solution (10 mL) of MB (10 mg L^{-1}) under UV- or visible-light illumination. A Phillips halogen lamp (50 W, GU5.3, 12 V) and a UV lamp (285 nm, 8 W) were used as the light sources for visible- and UV-light exposure, respectively. The photodegradation efficiency was monitored by measuring the absorption spectra at each 15 min interval up to 120 min. For cycling tests, the NR-based substrates can easily be separated from solutions and then be recycled by using simple washing with deionized water and absolute ethanol.

Acknowledgements

This work was supported by the Ministry of Science and Technology of the Republic of China under grant No: MOST 104-2112M-110-005.

Keywords: electron transfer · layered compounds · nanostructures · photocatalysis · photoluminescence

[1] J. Becker, K. R. Raghupathi, S. P. Jordan, K. Dan, T. Ranjit, *J. Phys. Chem. C* **2011**, *115*, 13844 – 13850.
[2] J. Schneider, M. Matsuoka, M. Takeuchi, J. Zhang, Y. Horiuchi, M. Anpo, D. W. Bahnemann, *Chem. Rev.* **2014**, *114*, 9919 – 9986.
[3] S. T. Kochuveedu, J. H. Oh, Y. R. Do, D. H. Kim, *Chem. Eur. J.* **2012**, *18*, 7467.
[4] C.-S. Wang, H.-Y. Lin, J.-M. Lin, Y.-F. Chen, *Appl. Phys. Express* **2012**, *5*, 062003.
[5] W.-J. Chen, J.-K. Wu, J.-C. Lin, S.-T. Lo, H.-D. Lin, D.-R. Hang, M. F. Shih, C.-T. Liang, Y. H. Chang, *Nanoscale Res. Lett.* **2013**, *8*, 313.
[6] Y. Y. Zhang, M. K. Ram, E. K. Stefanakos, D. Y. Goswami, *Surf. Coat. Technol.* **2013**, *217*, 119 – 123.
[7] Q. Wang, B. Geng, S. Wang, *Environ. Sci. Technol.* **2009**, *43*, 8968 – 8973.
[8] L. Sun, D. Zhao, Z. Song, C. Shan, Z. Zhang, B. Li, D. Shen, *J. Colloid Interface Sci.* **2011**, *363*, 175 – 181.
[9] Y. Chen, D. Zeng, K. Zhang, A. Lu, L. Wang, D.-L. Peng, *Nanoscale* **2014**, *6*, 874.
[10] M. Wu, W.-J. Chen, Y.-H. Shen, F.-Z. Huang, C.-H. Li, S.-K. Li, *ACS Appl. Mater. Interfaces* **2014**, *6*, 15052 – 15060.
[11] X. Liu, Z. Li, W. Zhao, C. Zhao, J. Yang, Y. Wang, *J. Colloid Interface Sci.* **2014**, *432*, 170 – 175.
[12] Y. J. Wang, Z. X. Wang, S. Muhammad, J. He, *CrystEngComm* **2012**, *14*, 5065 – 5070.
[13] N. Bao, L. Shen, T. Takata, K. Domen, *Chem. Mater.* **2008**, *20*, 110 – 117.
[14] S. Bai, J. Ge, L. Wang, M. Gong, M. Deng, Q. Kong, L. Song, J. Jiang, Q. Zhang, Y. Luo, Y. Xie, Y. Xiong, *Adv. Mater.* **2014**, *26*, 5689 – 5695.
[15] J. Low, S. Cao, J. Yu, S. Wageh, *Chem. Commun.* **2014**, *50*, 10768.
[16] a) Y. Li, H. Wang, S. Peng, *J. Phys. Chem. C* **2014**, *118*, 19842 – 19848; b) G. Zhang, H. Liu, J. Qu, J. Li, *Energy Environ. Sci.* **2016**, *9*, 1190.
[17] Y. He, L. Zhang, X. Wang, Y. Wu, H. Lin, L. Zhao, W. Weng, H. Wan, M. Fan, *RSC Adv.* **2014**, *4*, 13610.
[18] B. Hinnemann, P. G. Moses, J. Bonde, K. P. Jørgensen, J. H. Nielsen, S. Horch, I. Chorkendorff, J. K. Nørskov, *J. Am. Chem. Soc.* **2005**, *127*, 5308 – 5309.
[19] T. F. Jaramillo, K. P. Jørgensen, J. Bonde, J. H. Nielsen, S. Horch, I. Chorkendorff, *Science* **2007**, *317*, 100 – 102.
[20] L. Guardia, J. I. Paredes, J. M. Munuera, S. Villar-Rodil, M. Ayán-Varela, A. Martínez-Alonso, J. M. D. Tascón, *ACS Appl. Mater. Interfaces* **2014**, *6*, 21702 – 21710.

[21] D. Voiry, M. Salehi, R. Silva, T. Fujita, M. Chen, T. Asefa, V. B. Shenoy, G. Eda, M. Chhowalla, *Nano Lett.* **2013**, *13*, 6222 – 6227.
[22] S. Balendhran, J. Deng, J. Z. Ou, S. Walia, J. Scott, J. Tang, K. L. Wang, M. R. Field, S. Russo, S. Zhuiykov, M. S. Strano, N. Medhekar, S. Sriram, M. Bhaskaran, K. Kalantar-zadeh, *Adv. Mater.* **2013**, *25*, 109.
[23] X. K. Hu, Y. T. Qian, Z. T. Song, J. R. Huang, R. Cao, J. Q. Xiao, *Chem. Mater.* **2008**, *20*, 1527 – 1533.
[24] D. Xiang, C. Han, J. Zhang, W. Chen, *Sci. Rep.* **2014**, *4*, 4891.
[25] D.-R. Hang, K. H. Sharma, S. E. Islam, C. Chen, M. M. C. Chou, *Appl. Phys. Express* **2014**, *7*, 041101.
[26] D.-R. Hang, S. E. Islam, K. H. Sharma, S.-W. Kuo, C.-Z. Zhang, J.-J. Wang, *Nanoscale Res. Lett.* **2014**, *9*, 632.
[27] M. M. Y. A. Alsaifa, S. Balendhran, M. R. Field, K. Latham, W. Wlodarski, J. Z. Ou, K. Kalantar-zadeh, *Sens. Actuators B* **2014**, *192*, 196 – 204.
[28] X. Yu, G. Zhang, Z. Lu, J. Liu, X. Lei, X. Sun, *CrystEngComm* **2014**, *16*, 3935.
[29] K. Eda, *J. Solid State Chem.* **1992**, *98*, 350 – 357.
[30] S. Balendhran, S. Walia, H. Nili, J. Z. Ou, S. Zhuiykov, R. B. Kaner, S. Sriram, M. Bhaskaran, K. Kalantar-zadeh, *Adv. Funct. Mater.* **2013**, *23*, 3952 – 3970.
[31] J. Chen, M. Wang, X. Liao, Z. Liu, J. Zhang, L. Ding, L. Gao, Y. Li, *J. Alloys Compd.* **2015**, *619*, 406 – 410.
[32] M. M. Y. A. Alsaif, K. Latham, M. R. Field, D. D. Yao, N. Medehka, G. A. Beane, R. B. Kaner, S. P. Russo, J. Z. Ou, K. Kalantar-zadeh, *Adv. Mater.* **2014**, *26*, 3931 – 3937.
[33] M. A. Camacho-López, E. Haro-Poniatowski, L. Lartundo-Rojas, J. Livage, C. M. Julien, *Mater. Sci. Eng. B* **2006**, *135*, 88 – 94.
[34] R. Murugan, A. Ghule, C. Bhongale, H. Chang, *J. Mater. Chem.* **2000**, *10*, 2157 – 2162.
[35] D.-R. Hang, S. E. Islam, K. H. Sharma, C. Chen, C.-T. Liang, M. M. C. Chou, *Semicond. Sci. Technol.* **2014**, *29*, 085004.
[36] X. H. Wang, J. G. Li, H. Kamiyama, Y. Moriyoshi, T. Ishigaki, *J. Phys. Chem. B* **2006**, *110*, 6804 – 6809.
[37] S. B. Rawal, S. Bera, D. Lee, D.-J. Jang, W. I. Lee, *Catal. Sci. Technol.* **2013**, *3*, 1822 – 1830.
[38] T. T. Li, L. H. Zhao, Y. M. He, J. Cai, M. F. Luo, J. J. Lin, *Appl. Catal. B* **2013**, *129*, 255 – 263.
[39] L. Ge, C. C. Han, J. Liu, *Appl. Catal. B* **2011**, *108*, 100 – 107.
[40] W. Liu, M. Wang, C. Xu, S. Chen, X. Fu, *J. Mol. Catal. A* **2013**, *368 – 369*, 9 – 15.
[41] W. Liu, M. Wang, C. Xu, S. Chen, X. Fu, *Mater. Res. Bull.* **2013**, *48*, 106 – 113.

Received: May 6, 2016
Published online on ■■ ■■, 0000

FULL PAPER

2D nanoflakes: Nanometer-thick molybdenum oxide flakes were employed as a co-catalyst for ZnO nanorods to enhance their photocatalytic performance (see figure; CB = conductive band, VB = valence band, MB = methylene blue). The recombination of photogenerated electrons and holes is suppressed by the double charge-transfer mechanism.

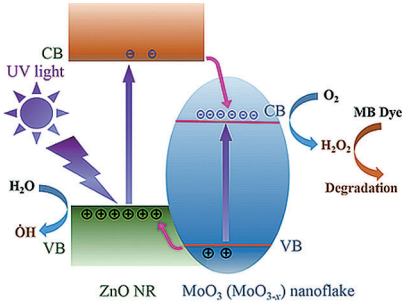

Photocatalysis

D.-R. Hang, K. H. Sharma, C.-H. Chen, S. E. Islam*

■■ – ■■

Enhanced Photocatalytic Performance of ZnO Nanorods Coupled by Two-Dimensional α-MoO_3 Nanoflakes under UV and Visible Light Irradiation